Using multi-angle WorldView-2 imagery to determine bathymetry near Oahu, Hawaii

Krista R. Lee*, Richard C. Olsen, Fred A. Kruse, Angela M. Kim
Department of Physics and Remote Sensing Center
Naval Postgraduate School, 833 Dyer Road, Monterey, California, 93943, USA

ABSTRACT

Multispectral imaging (MSI) data collected at multiple angles over shallow water provide analysts with a unique perspective of bathymetry in coastal areas. Observations taken by DigitalGlobe's WorldView-2 (WV-2) sensor acquired at 39 different view angles on 30 July 2011 were used to determine the effect of acquisition angle on bathymetry derivation. The site used for this study was Kailua Bay (on the windward side of the island of Oahu). Satellite azimuth and elevation for these data ranged from 18.8 to 185.8 degrees and 24.9 (forward-looking) to 24.5 (backward-looking) degrees (respectively) with 90 degrees representing a nadir view. Bathymetry were derived directly from the WV-2 radiance data using a band ratio approach. Comparison of results to LiDAR-derived bathymetry showed that varying view angle impact the quality of the inferred bathymetry. Derived and reference bathymetry have a higher correlation as images are acquired closer to nadir. The band combination utilized for depth derivation also has an effect on derived bathymetry. Four band combinations were compared, and the Blue & Green combination provided the best results.

Keywords: Multispectral imaging, WorldView-2, bathymetry derivation, multi-angle imagery

1. INTRODUCTION

Imagery data acquired from satellites are useful in the field of oceanography. Information about shallow water bathymetry is beneficial to scientists or groups that require knowledge of ocean depths in a particular coastal location. The use of MSI data has been shown to adequately determine depths of remote coastal areas, as SOund Navigation and Ranging (SONAR) or Light Detection and Ranging (LiDAR) soundings or other bathymetric data may not be available.

The purpose of this research was to integrate the use of multiple satellite image acquisition angles over one location, and determine what role these varying angles play in bathymetric depth determination. Analyses of 39 WorldView-2 images acquired over Kailua Bay on the windward side of Oahu, Hawaii were used to reach a conclusion about the accuracy of bathymetric derivation from MSI.

Portions of this work were previously published in Lee *et al*. (2012)[1]. Additional research results are included in this paper, which summarizes complete results from Lee (2012)[2].

2. BACKGROUND

2.1 WV-2 satellite

DigitalGlobe's third operational satellite, WV-2, is capable of capturing 1.85 m multispectral (and 0.46 m panchromatic) spatial resolution at nadir. WV-2 has 9 spectral bands – one panchromatic (PAN), ranging from approximately 450 to 800 nm (centered at 632 nm), and 8 multispectral (MS) bands, ranging from approximately 400 to 1050 nm. These MS bands include: Coastal (centered at 427 nm), Blue (centered at 478 nm), Green (centered at 546 nm), Yellow (centered at 608 nm), Red (centered at 659 nm), Red Edge (centered at 724 nm), NIR-1 (centered at 831 nm), and NIR-2 (centered at 908 nm)[3]. Refer to Figure 1.

* E-mail: krista.r.lee@gmail.com

Algorithms and Technologies for Multispectral, Hyperspectral, and Ultraspectral Imagery XIX,
edited by Sylvia S. Shen, Paul E. Lewis, Proc. of SPIE Vol. 8743, 874311 · © 2013 SPIE
CCC code: 0277-786X/13/$18 · doi: 10.1117/12.2015660

Downloaded From: http://proceedings.spiedigitallibrary.org/ on 05/27/2017 Terms of Use: http://spiedigitallibrary.org/ss/termsofuse.aspx

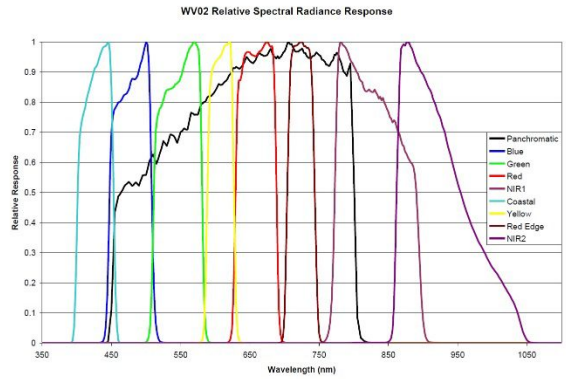

Figure 1. WV-2's relative spectral radiance response[4]

The WV-2 sensor's 8 MS bands are arranged in two arrays of 4 MS bands each (MS1 and MS2). MS1 includes Blue, Green, Red, and NIR-1. MS2 is comprised of Coastal, Yellow, Red Edge, and NIR-2. Imaging options include: PAN only, PAN + MS1, and PAN + 8 MS (MS1 and MS2)[3]. There is a 0.3 second delay between MS1 and MS2 acquisitions, according to G. Miecznik (unpublished data, 2012).

When combined, these bands are designed to improve the segmentation and classification of land and aquatic features beyond any other multispectral satellite imager. After WV-2's launch, it was speculated that the increased agility and addition of the Coastal band would improve remote bathymetric measurements (mainly due to the Coastal band's wavelength value, making it least absorptive by water). Analysts expected to be able to calculate depths up to 20 meters, and possibly even 30 meters using the Coastal, Blue, and Green bands. Once scientists were able to utilize WV-2 imagery, the Coastal band has proven to be useful for the retrieval of water depth, true-color correction for human vision representation, chlorophyll absorption, and atmospheric scattering correction[5, 6].

2.2 WV-2 multi-angle capabilities

Multi-angle remote sensing capabilities offer a number of advantages with respect to a single shot dataset. Multi-angular data fusion has been shown to allow the exploitation/investigation of the bidirectional reflectance distribution function (BRDF), the extraction of digital height maps (DHMs), atmospheric parameter retrieval, and improvements in classification[7].

There is significant improvement shown over the baseline classification when using a multi-angle WV-2 sequence. In terms of spatial classification, Longbotham *et al.* (2011) successfully demonstrated the ability to differentiate between classes like bridges and man-made structures, which are generally difficult to classify because they are spectrally similar to ground-level classes of the same material. Improvements in terms of spectral classification were also made using multi-angle data[8, 9].

2.2.1 WV-2 imagery dataset used in this research

A collection of 39 MS images of the windward side of Oahu, Hawaii was acquired by WV-2 on 30 July 2011 between 21:22:49Z and 21:28:54Z. Images were acquired at approximately 10 second intervals, and were collected for just over 6 minutes. Mean satellite elevation angles range from 24.9 degrees (most forward-looking) to 77.8 degrees (most nadir) to 24.5 degrees (most backward-looking), assuming that 90 degrees represents a nadir view.

2.3 Study site: Kailua Bay, Oahu, Hawaii

This study focused on Kailua Bay, located on the windward side of the Oahu coastline of Hawaii (Figure 2). The bay's approximate latitude/longitude is: 21 degrees 24' 29" N, 157 degrees 44' 09" W. This particular beach was chosen because it was the least cloudy area from the 39 WV-2 images in the acquired dataset.

Downloaded From: http://proceedings.spiedigitallibrary.org/ on 05/27/2017 Terms of Use: http://spiedigitallibrary.org/ss/termsofuse.aspx

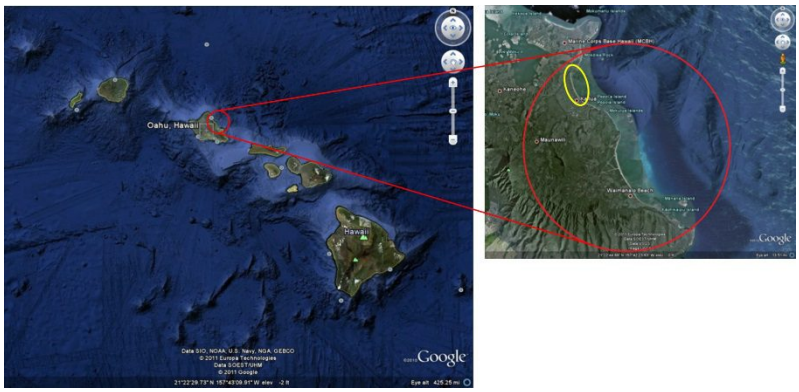

Figure 2. The Hawaiian Islands (left), focusing on Kailua Bay, Oahu (right) (From Google Earth)

Kailua Bay is a carbonate reef-dominated embayment. There are two categories of benthic substrate found here: areas of carbonate sand and fossil reef hardgrounds, and reef habitats of coral and algae species. There is a sand-floored channel at the center of the bay, which cuts across the reef and connects the seaward and nearshore sand fields. Algae and corals grow on the plains[10].

Areas with sand and fossil reef appear light-colored and are highly reflective in the WV-2 imagery. The coral and algae communities look dark and have low reflectance[10].

3. METHODS

3.1 Initial data preparation

A number of pre-processing steps were performed before bathymetric derivation could occur. Images were first mosaicked and analyzed for overall quality and cloud cover. Map coordinate conversion, radiance calibration, land/cloud mask creation, sun glint removal, and the application of a ratio method for bathymetry derivation followed.

Once images had been mosaicked and analyzed for overall quality and cloud cover, they were converted from latitude/longitude to Universal Transverse Mercator (UTM), World Geodetic System 1984 (WGS84), Zone 4N with square pixels. Scenes were then ordered by mean satellite elevation angle (most forward-looking to most nadir to most backward-looking). Figure 3 shows five out of 39 images, after the performance of pre-processing steps, as acquired by WV-2.

Downloaded From: http://proceedings.spiedigitallibrary.org/ on 05/27/2017 Terms of Use: http://spiedigitallibrary.org/ss/termsofuse.aspx

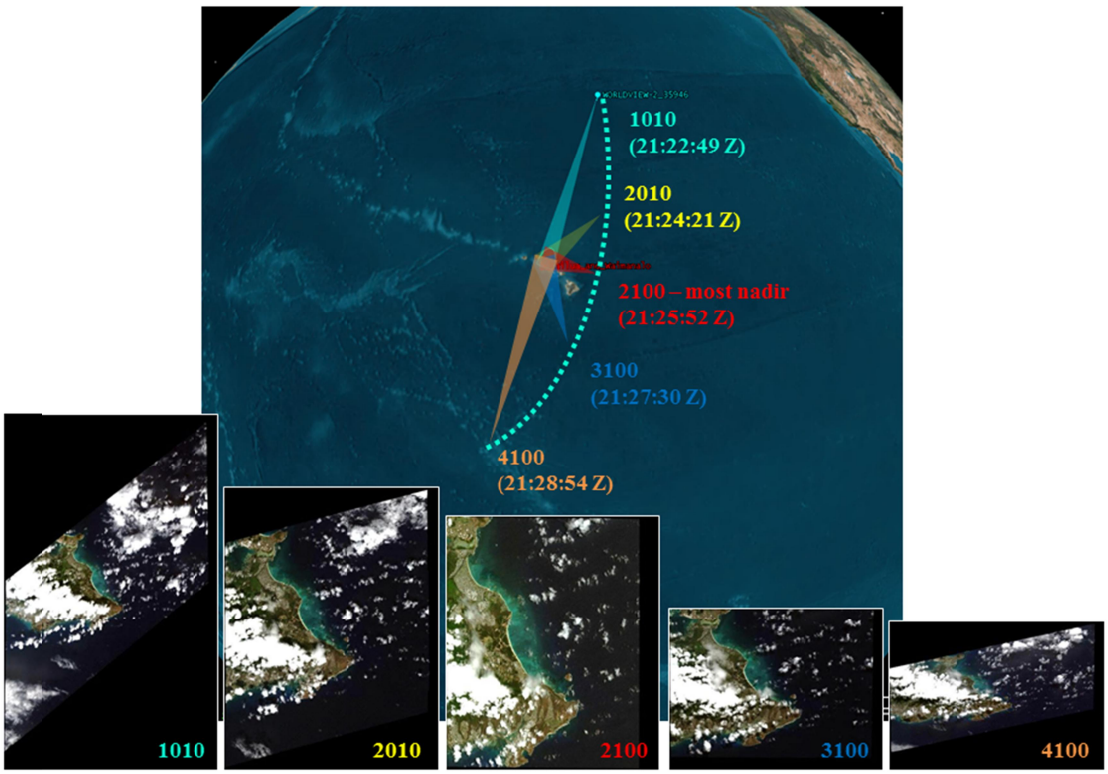

Figure 3. Five example images out of the 39 WV-2 image acquisitions (labels correspond to actual Image IDs)

3.2 Radiance calibration

The WV-2 spectral radiance response is defined as the ratio of the number of photo-electrons measured by the system, to the spectral radiance [$W\text{-}m^{-2}\text{-}sr^{-1}\text{-}\mu m^{-1}$] at a certain wavelength present at the entrance to the telescope aperture. The spectral radiance response for each band is normalized by dividing by the maximum response value for that band to arrive at a relative spectral radiance response[11].

Relative radiometric calibration and correction are necessary. This is because a uniform scene does not create a uniform image when it comes to raw digital numbers (DNs). This type of correction minimizes image artifacts, such as vertical streaks or bands due to differences in gain or offset, and is performed on raw data from all detectors in all bands during the early stages of WV-2 product generation. The products are linearly scaled to absolute spectral radiance[11].

In the case of large mosaics, radiometric balancing will help match the brightness of the other scenes used in the mosaic[11]. As glint removal is performed on images after the radiance calibration step, all images were left in radiance for this research.

3.3 Data subsetting and image registration

Images were subset to focus on Kailua Bay. This was done to reduce file sizes, emphasize one geographic location with interesting and varying bathymetry, as well as to better concentrate on one spot with less cloud cover.

All non-nadir images were registered to the most nadir image by interactively selecting 20 tie points for the same locations in the non-nadir images. The data were then warped using a first order polynomial. Maximum pixel error for the registrations was 1.521 pixels with an average root mean square (RMS) error of approximately 0.895 pixels for the entire dataset. Images were then chipped so that every scene covered the same geographic coordinates and were 995 samples by 999 lines (Figure 4).

Downloaded From: http://proceedings.spiedigitallibrary.org/ on 05/27/2017 Terms of Use: http://spiedigitallibrary.org/ss/termsofuse.aspx

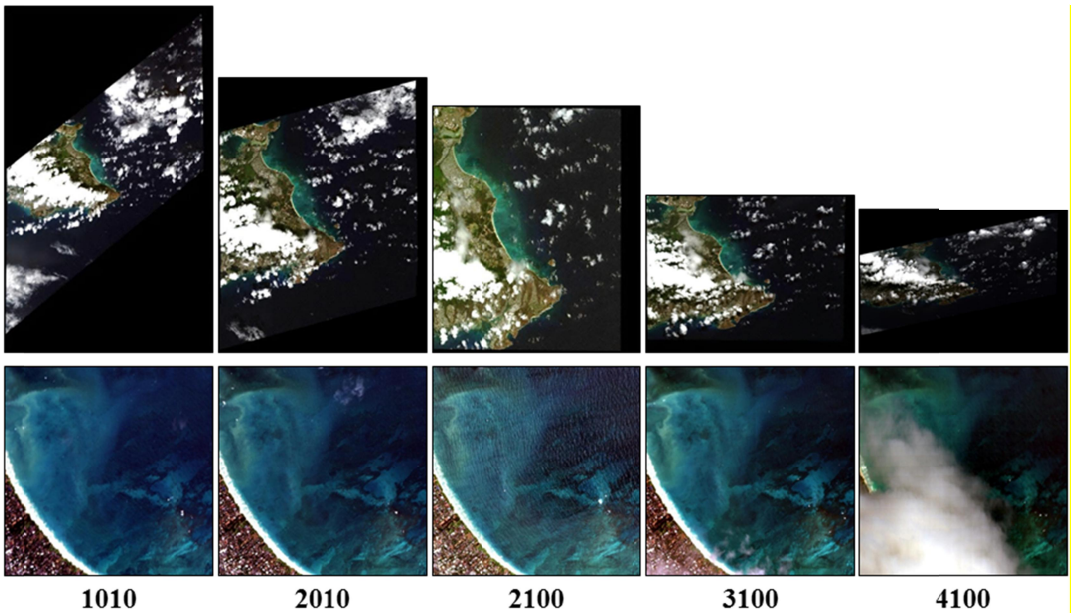

Figure 4. After registration, each image (top row) was chipped to the 995 x 999 pixel scene shown (bottom row)

3.4 Land, glint, cloud, and whitecap masks and glint removal

Areas that needed to be masked were determined by using scatter plots that compared the Blue and NIR-1 bands. The scatter plots classified land, glint, clouds, and whitecaps as any pixels with values greater than the user-defined points chosen within the plot. Every other pixel would, therefore, be considered not land, glint, clouds, or whitecaps and would not be masked (Figure 5). Figure 6 illustrates how Figure 5's user-defined region affects the imagery.

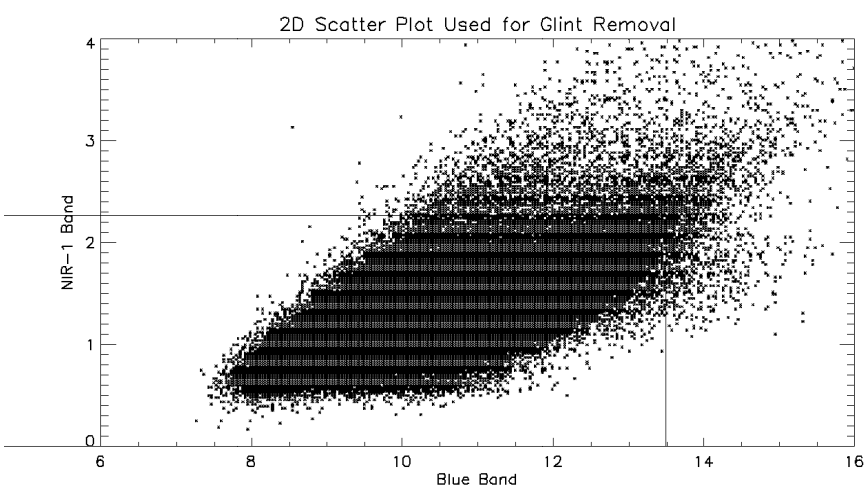

Figure 5. 2D scatter plot of Blue vs. NIR-1 bands; the user-defined outline region includes pixels containing water, and everything else can generally be classified as land, clouds, glint, whitecaps, etc. (e.g., not water)

Downloaded From: http://proceedings.spiedigitallibrary.org/ on 05/27/2017 Terms of Use: http://spiedigitallibrary.org/ss/termsofuse.aspx

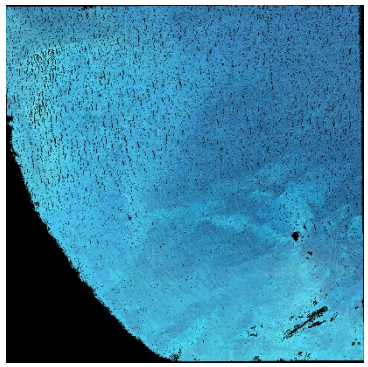

Figure 6. Land, glint, clouds, and whitecaps have been masked in this image

The method used for glint removal was based on the method revised by Hedley *et al.* (2005) after Hochberg *et al.* (2003), and was applied to two WV-2 bands at a time. The following band combinations were analyzed:

(1) Coastal & Blue,
(2) Coastal & Green,
(3) Blue & Green, and
(4) Green & Yellow.

Work by Hedley *et al.* (2005) established the linear relationship between near infrared (NIR) and visible (VIS) bands using a linear regression based on a sample of the image pixels. Over areas with underlying spectral brightness, such as deep water, one or more regions with a range of sun glint are selected. For each VIS band, all selected pixels are included in a linear regression of NIR brightness (x-axis) against the VIS band brightness (y-axis). If the slope of this line for band i is b_i, then all the pixels in the image can be deglinted in band i by applying Equation 1:

$$R'_i = R_i - b_i(R_{\mathrm{NIR}} - \mathrm{Min}_{\mathrm{NIR}}), \tag{1}$$

which means: reduce the pixel value in band i (R_i) by the product of the regression slope (b_i) and the difference between the pixel NIR value (R_{NIR}) and the ambient NIR level ($\mathrm{Min}_{\mathrm{NIR}}$). R'_i is the sun glint corrected pixel brightness in band i. $\mathrm{Min}_{\mathrm{NIR}}$ represents the NIR brightness of a pixel with zero sun glint, and can be estimated by the minimum NIR found in the regression sample or as the minimum NIR value found in the entire image[12, 13].

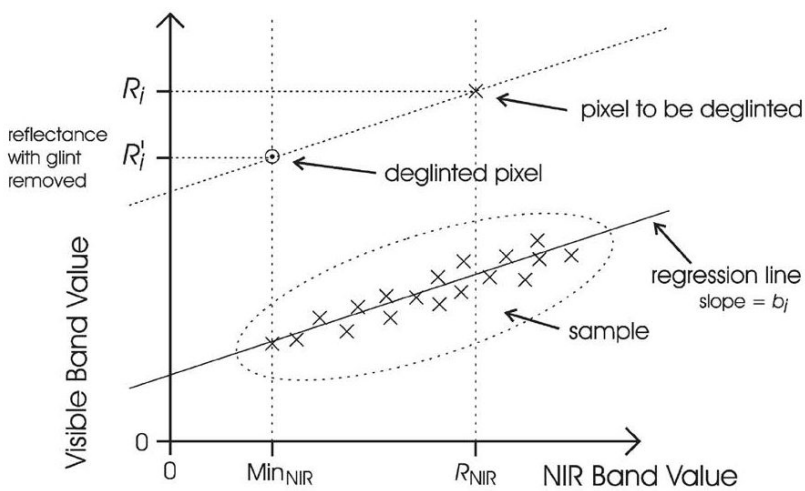

Figure 7. Graphical interpretation of the Hedley *et al.* (2005) de-glinting method[12]

The analysis incorporates the slope of the regression line. Equations 2 and 3 represent simplified examples of the modified equations used in the code:

Downloaded From: http://proceedings.spiedigitallibrary.org/ on 05/27/2017 Terms of Use: http://spiedigitallibrary.org/ss/termsofuse.aspx

$$\text{Green} = \text{Green} - \text{Slope of Green Regression Line} * (\text{NIR-1} - \text{MinNIR-1}) \quad (2)$$

$$\text{Yellow} = \text{Yellow} - \text{Slope of Yellow Regression Line} * (\text{NIR-2} - \text{MinNIR-2}) \quad (3)$$

There are, however, a number of differences between the Hedley *et al.* (2005) method and the one used for this research. This code utilized only two of the six possible WV-2 VIS bands at one time. It also focused on the entire, global scene rather than a small, local portion (only deep water, for example). It also incorporated masking, which was not used in the Hedley *et al.* (2005) research.

3.5 Relative and derived bathymetry derivation using a band ratio transform

A two-step process was used to derive bathymetry. Relative bathymetry was determined by performing a band ratio method, and then derived bathymetry values were obtained by regressing relative bathymetry values against verified depth data.

The relative bathymetric values in this research were extracted using Equation 4, with a slight adjustment to the constant value used by Camacho (2006)[14]:

$$\ln(100 * b1) / \ln(100 * b2) \quad (4)$$

where b1 is the first band used, and b2 is the second. This is also a modification of the equation used by Stumpf *et al.* (2003)[15].

Bathymetry data of Kailua Bay were acquired from the University of Hawaii at Manoa, School of Ocean & Earth Science & Technology, Department of Geology and Geophysics (data are available at http://www.soest.hawaii.edu/coasts/data/oahu/shoals.html and information about this dataset is available at http://www.soest.hawaii.edu/coasts/data/readme.html#shoals) in shapefile format. According to the University of Hawaii website, these data were collected from the SHOALS website as part of a survey conducted in 2000 (information is available at http://shoals.sam.usace.army.mil/hawaii/pages/Oahu.htm). After investigating the origins of the dataset, however, and determining that these data were not collected by SHOALS in 2000, it is now believed that the data were collected by USGS circa 2002 to 2005. This information was provided by C. Fletcher (unpublished data, 2012). Prior to the completion of this particular project, there was no resolution concerning the actual details about the dataset. Despite this, the available data were converted to a raster in the proper map projection, geographically linked to the image chip, and then clipped to the 995 by 999 pixels size. These data were then used as the "true" data.

Derived depth values were calculated by regressing the relative depth values with the actual depth values collected by the "true" bathymetry. The chi-squared and correlation values helped determine the "goodness of fit." A low chi-squared value is indicative of a better fit. Correlation values are interpreted as percentages, so the highest value represents the best fit.

4. RESULTS

4.1 Bathymetry from the entire image

The effects of collection geometry on water depth derivation were analyzed by running all 39 images through the processing and analysis approach described above. Chi-squared and correlation values were recorded, and images of derived depth versus actual "true" depth plots were compared. The "true" bathymetry data are shown in Figure 8.

Downloaded From: http://proceedings.spiedigitallibrary.org/ on 05/27/2017 Terms of Use: http://spiedigitallibrary.org/ss/termsofuse.aspx

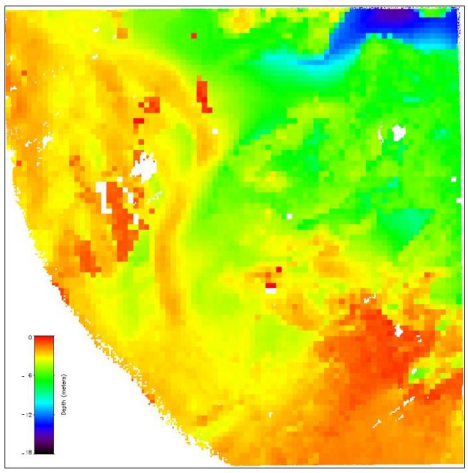

Figure 8. "True" bathymetry data; depth is represented by the Rainbow scale (shallow water is red and deep water is black)

The results of the regression were the derived depth values. These were scaled to meters and plotted. Derived depth plots from Image IDs 1010 (most forward-looking), 2010, 2100 (most nadir), 3100, and 4100 (most backward-looking) are shown in Figure 9 for each band combination. All images have the same scale, a range of depths from 0 m (red) to -18 m (black).

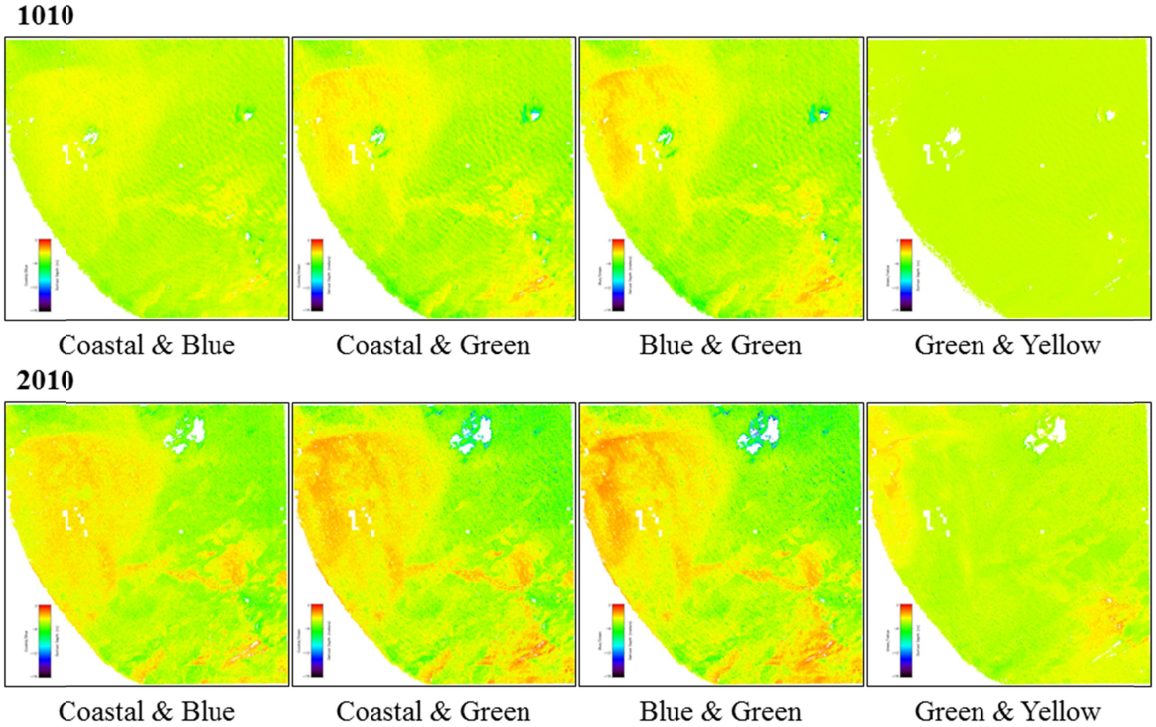

Downloaded From: http://proceedings.spiedigitallibrary.org/ on 05/27/2017 Terms of Use: http://spiedigitallibrary.org/ss/termsofuse.aspx

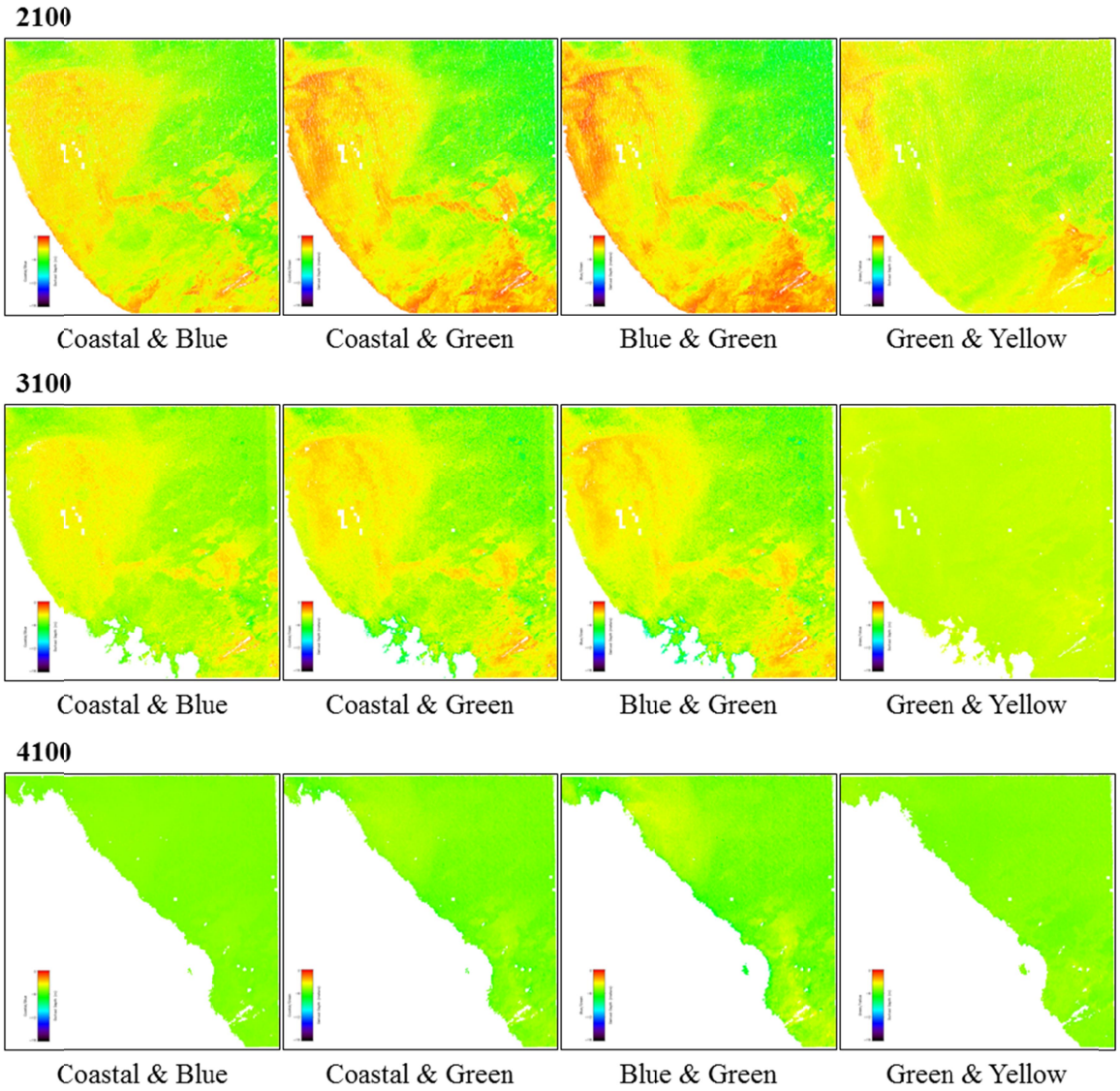

Figure 9. Derived depths for each band combination for Image IDs 1010, 2010, 2100, 3100, and 4100

None of these derived depth maps come close to a perfect correlation to the "true" bathymetry data. This most likely has to do with a number of factors, including high off-nadir acquisition angle and also cloud cover (seen as white, masked data in Image IDs 3100 and 4100). Due to the fact that wave patterns can be seen in the derived depth images, it is also speculated that a better glint removal method may be required in order to derive more accurate depths.

Upon closer inspection, the Coastal & Green and Blue & Green WV-2 band combinations appear to perform better. Also, derived depth more closely matches "true" depth as the sensor is acquiring images closer to nadir.

4.2 Variation in acquisition angles

Plots of derived depth versus "true" depth for Image IDs 1010, 2010, 2100, 3100, and 4100 were created and compared so as to gain a better understanding of the effect of acquisition angle on depth determination. The chi-squared and correlation values of each band combination were determined and are displayed for Image ID 2100 (most nadir) in Figure 10.

Downloaded From: http://proceedings.spiedigitallibrary.org/ on 05/27/2017 Terms of Use: http://spiedigitallibrary.org/ss/termsofuse.aspx

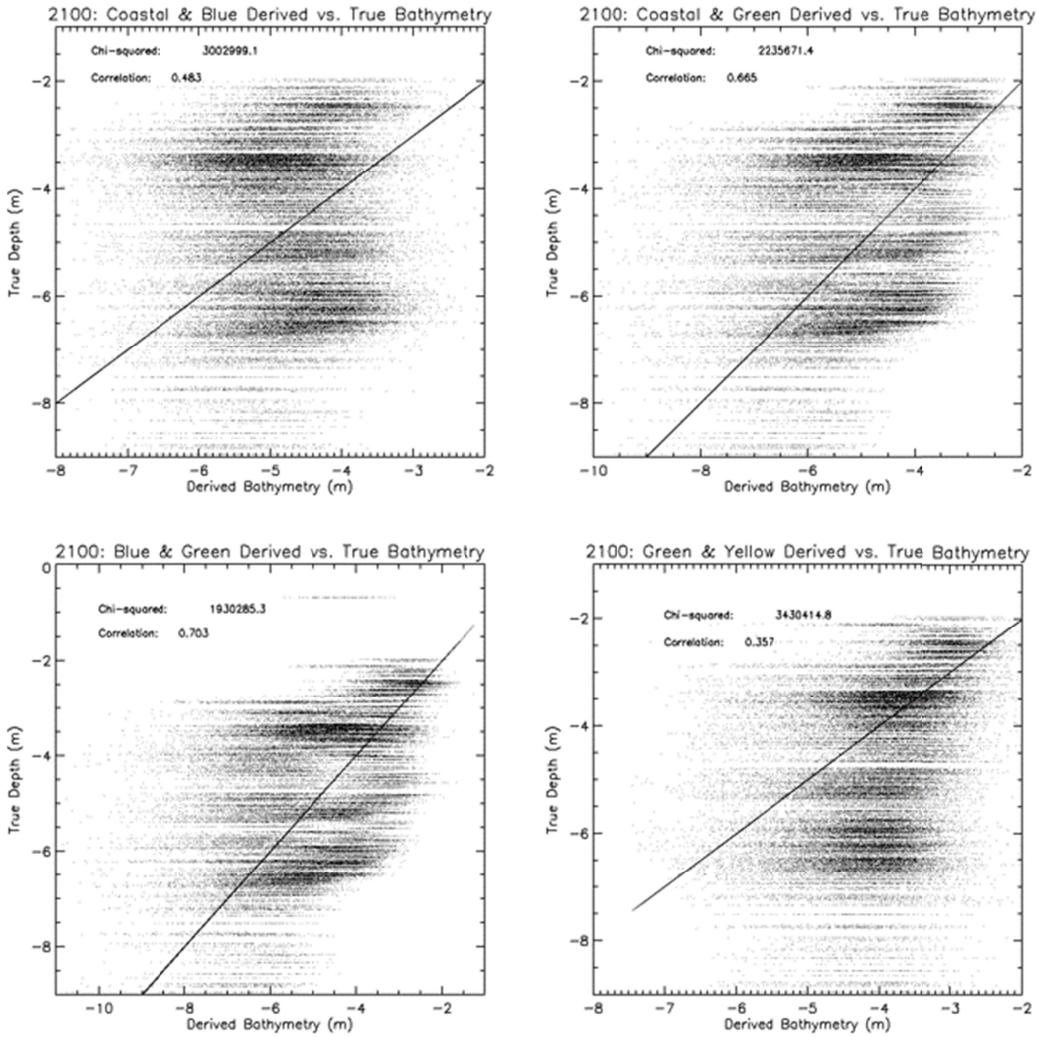

Figure 10. Derived depth vs. "true" depth for Image 2100 (most nadir) for all band combinations

Chi-squared and correlation values were also calculated and plotted for each Image ID for all four band combinations. These values represent the correlation of the depth derived from the band combination ratio versus the "true" depth. Results are shown in Figures 11 through 14.

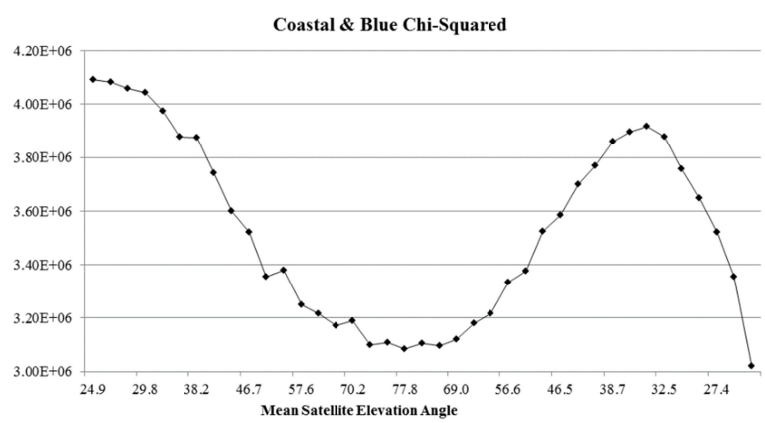

Downloaded From: http://proceedings.spiedigitallibrary.org/ on 05/27/2017 Terms of Use: http://spiedigitallibrary.org/ss/termsofuse.aspx

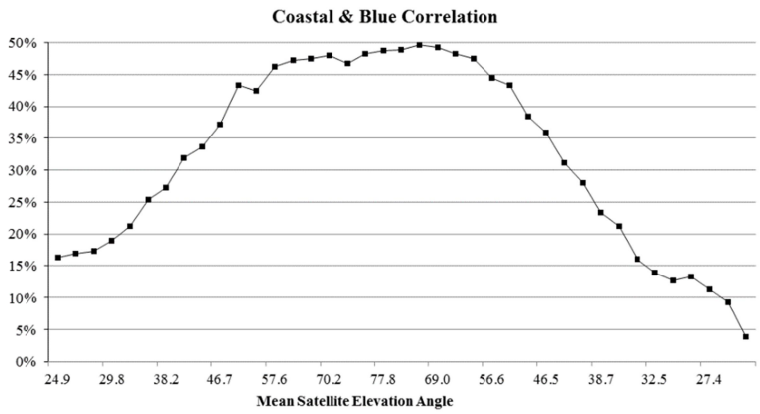

Figure 11. Coastal & Blue: Chi-squared (top) and correlation (bottom) values (y-axis) plotted against the mean satellite elevation angle (x-axis) for all 39 WV-2 images

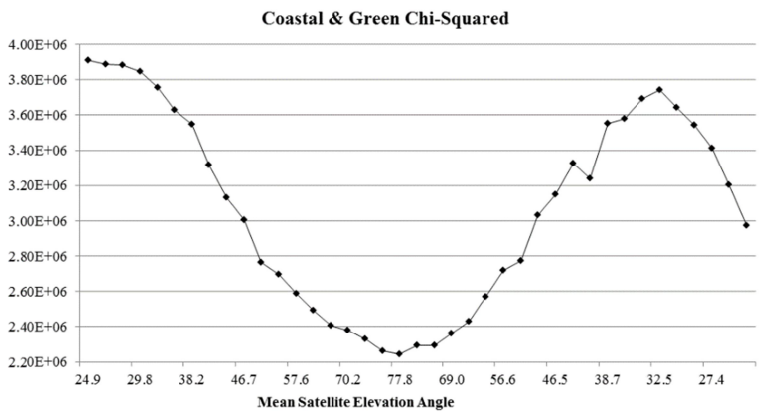

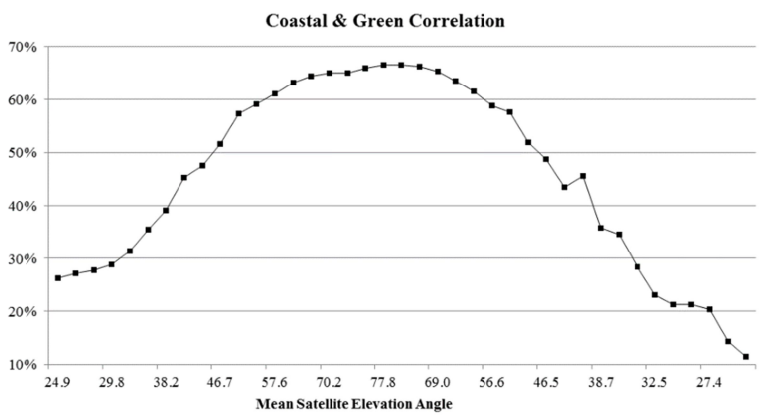

Figure 12. Coastal & Green: Chi-squared (top) and correlation (bottom) values (y-axis) plotted against the mean satellite elevation angle (x-axis) for all 39 WV-2 images

Downloaded From: http://proceedings.spiedigitallibrary.org/ on 05/27/2017 Terms of Use: http://spiedigitallibrary.org/ss/termsofuse.aspx

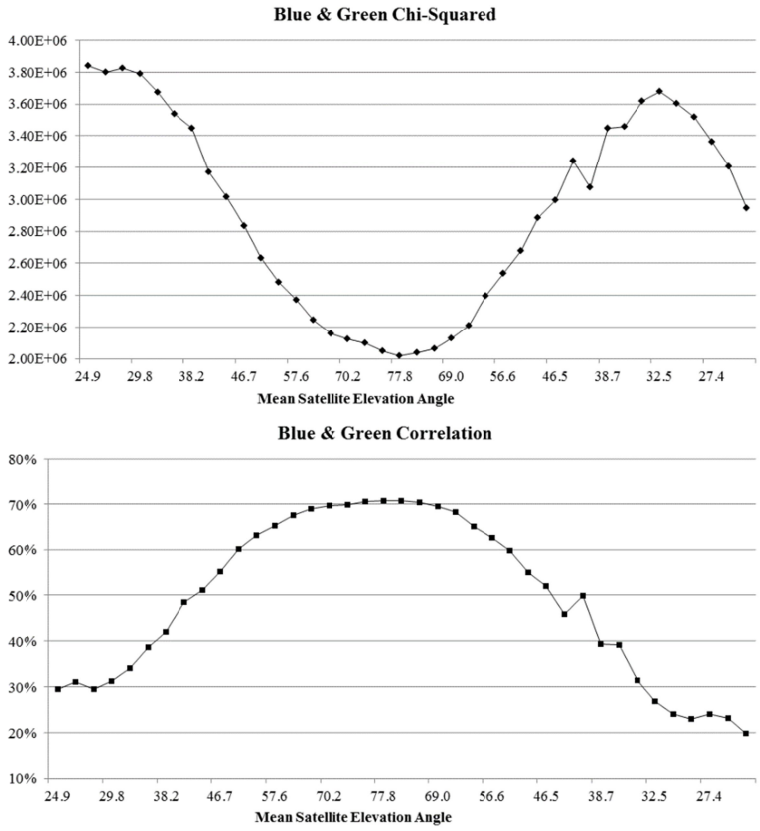

Figure 13. Blue & Green: Chi-squared (top) and correlation (bottom) values (y-axis) plotted against the mean satellite elevation angle (x-axis) for all 39 WV-2 images

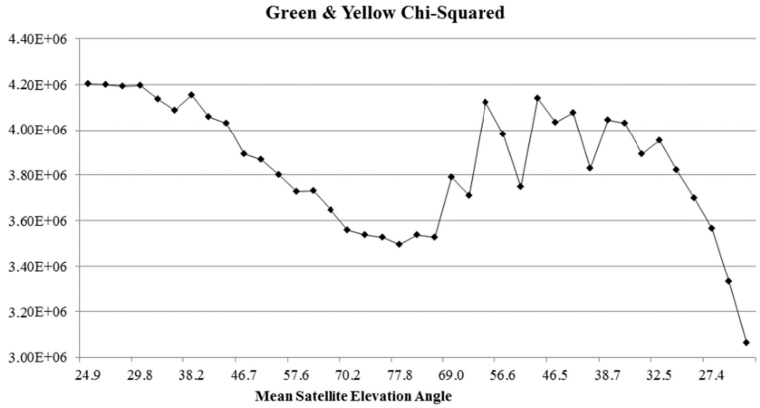

Downloaded From: http://proceedings.spiedigitallibrary.org/ on 05/27/2017 Terms of Use: http://spiedigitallibrary.org/ss/termsofuse.aspx

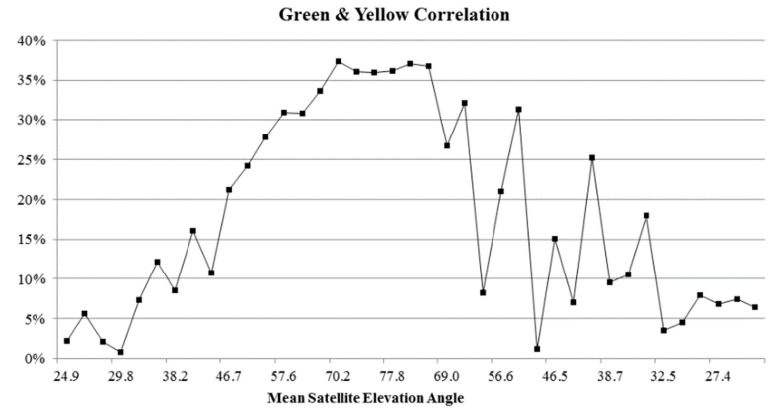

Figure 14. Green & Yellow: Chi-squared (top) and correlation (bottom) values (y-axis) plotted against the mean satellite elevation angle (x-axis) for all 39 WV-2 images

For the four band combinations tested, those images that were acquired closer to nadir had the lowest chi-squared values and the highest correlations. The optimal values were found when running the Blue & Green code, with a correlation value around 71%. The most erratic results came from the Green & Yellow code, perhaps because the Yellow band did not penetrate as deeply into the water.

Low chi-squared values were also seen from Image IDs 4050 to 4100. This is possibly due to the fact that clouds were entering the scene, being masked and, therefore, leaving very little water from which to collect spectral information for depth derivation.

5. CONCLUSIONS

Thirty-nine WV-2 images collected at multiple angles over a coastal, shallow water environment were used to analyze the effect of varying view angle on bathymetry derivation. Following initial data preparation steps, the entire dataset was analyzed to determine what effect, if any, acquisition angle has on nearshore depth retrieval. The data processing and analysis consisted of radiance calibration, steps to remove sun glint, a band ratio method to determine relative depth, and a regression to find derived depth.

Accuracy of depth retrieval did, in fact, demonstrate an association with image acquisition angle. Images acquired at more off-nadir view angles proved to have lower correlation values to the actual "true" bathymetry data. This was shown by the increase in correlation values for more nadir images within the dataset, followed by a decrease as images became more backward-looking. Likewise, chi-squared values decreased as the code approached the nadir-looking images, and increased again after that.

Four band combinations were compared in an effort to determine which WV-2 bands might be best for determining depth in shallow, coastal environments. These included: Coastal & Blue, Coastal & Green, Blue & Green, and Green & Yellow. Of the four, the Blue & Green band combination performed best, with the highest correlation value of approximately 71% between "true" and derived depth.

The results of this research showed that more accurate bathymetric depths will be derived from images that have been acquired closer to nadir viewing geometry. Additionally, when using imagery from the WV-2 sensor, a combination of the Blue and Green bands will penetrate into the water in such a way that a higher accuracy of depth information will be obtained.

6. FUTURE WORK

There are a number of factors that may have negatively affected the data and analysis. While the scene over Kailua Bay was chosen because it was the least cloudy beach out of the 39 images in the dataset, it still had cloud cover (especially between Image IDs 4050 and 4100). This led to fewer data points that could be analyzed for those scenes. It would also

Downloaded From: http://proceedings.spiedigitallibrary.org/ on 05/27/2017 Terms of Use: http://spiedigitallibrary.org/ss/termsofuse.aspx

have been preferable to have used a more recent dataset for "true" bathymetry. This particular collection is thought to have been acquired between 2002 and 2005, and in an environment as dynamic as a coastal shoreline, bathymetry could have changed significantly. In the future, it would be advantageous to find a recent bathymetric dataset, and then acquire WV-2 data over that geographic location.

There are a number of possibilities for improvement and growth in future research related to this particular topic. It would be beneficial to apply the analysis approach to the entire dataset scene, rather than just the image chips. It would also be interesting to use a dataset with a wider range of satellite elevation angles (more off-nadir to more nadir and back). It might also be fascinating to apply this method to nearshore areas with black sand to see whether or not sand color affects the results of the algorithm.

REFERENCES

[1] Lee, K. R., Olsen, R. C., Kruse, F. A., "Using multi-angle WorldView-2 imagery to determine ocean depth near the island of Oahu, Hawaii," Proc. SPIE (2012).

[2] Lee, K. R., "Using multi-angle WorldView-2 imagery to determine ocean depth near Oahu, Hawaii," Unpublished M.S. Thesis, Naval Postgraduate School, Monterey, CA, http://nps.edu/Academics/Centers/RSC/documents/12Sep_Lee.pdf (2012).

[3] DigitalGlobe, Inc., "WorldView-2," http://www.digitalglobe.com/about-us/content-collection#satellites&worldview-2 (2012).

[4] DigitalGlobe, Inc., "Spectral Response for DigitalGlobe WorldView 1 and WorldView 2 Earth Imaging Instruments," http://www.digitalglobe.com/downloads/DigitalGlobe_Spectral_Response.pdf (2011).

[5] Pacifici, F., Navular, K., "Very High Spatial Resolution Imagery for Urban Application," http://www.earthzine.org/2011/06/27/very-high-spatial-resolution-imagery-for-urban-applications/ (2011).

[6] Marchisio, G., Pacifici, F., and Padwick, C., "Coastal applications of WorldView-2 high resolution multispectral imagery," paper presented at American Society for Photogrammetry and Remote Sensing, Milwaukee, WI USA (2011).

[7] Pacifici, F., Chanussot, J., Du, Q., "2011 GRSS Data Fusion Contest: Exploiting WorldView-2 Multi-Angular Acquisitions," presented at IGARSS 2011, (http://www.grss-ieee.org/wp-content/uploads/lectures/igarss2011_2tu1_5_pacifici/start.html) (2011).

[8] Longbotham, N., Chaapel, C., Bleiler, C., Bleiler, L., Padwick, C., Emery, W.J., Pacifici, F., "Very High Resolution Multiangle Urban Classification Analysis," IEEE Transactions on Geoscience and Remote Sensing, Vol. 99, 1-16 (2011).

[9] Longbotham, N., Bleiler, C., Chaapel, C., Padwick, C., Emery, W., and Pacifici, F., "Spatial Classification of WorldView-2 Multi-angle Sequence," paper presented at Joint Urban Remote Sensing Event, Munich, Germany (2011).

[10] Isoun, E., Fletcher, C.H., Frazer, N., Gradie, J., "Multi-spectral mapping of reef bathymetry and coral cover; Kailua Bay, Hawaii," Coral Reefs, 22, 68-82 (2003).

[11] Updike, T., Comp, C., "Radiometric Use of WorldView-2 Imagery," Technical Note, DigitalGlobe, Inc., Revision 1.0 (http://www.digitalglobe.com/downloads/Radiometric_Use_of_WorldView-2_Imagery.pdf) (2010).

[12] Hedley, J. D., Harborne, A. R., and Mumby, P. J., "Simple and robust removal of sun glint for mapping shallow-water benthos, Int. J. Remote Sens., 26(10), 2107 (2005).

[13] Hochberg, E. J., Andrefouet, S., and Tyler, M. R., "Sea Surface Correction of High Spatial Resolution Ikonos Images to Improve Bottom Mapping in Near-Shore Environments," IEEE Trans. Geosci. Remote Sens., 41, 1724 (2003).

[14] Camacho, M. A., "Depth analysis of Midway Atoll using QuickBird multi-spectral imaging over variable substrates," Unpublished M.S. Thesis, Naval Postgraduate School, Monterey, CA (2006).

[15] Stumpf, R.P., Holderied, K., Sinclair, M., "Determination of water depth with high-resolution satellite imagery over variable bottom types," Limnol. Oceanogr., 48(1, part 2), 547-556 (2003).

Downloaded From: http://proceedings.spiedigitallibrary.org/ on 05/27/2017 Terms of Use: http://spiedigitallibrary.org/ss/termsofuse.aspx